



## Article

**Cite this article:** Gurung TR, Kayastha RB, Fujita K, Joshi SP, Sinisalo A, Kirkham JD (2022). A long-term mass-balance reconstruction (1974–2021) and a decadal in situ mass-balance record (2011–2021) of Rikha Samba Glacier, central Himalaya. *Journal of Glaciology* 1–14. <https://doi.org/10.1017/jog.2022.93>

Received: 21 July 2021

Revised: 14 September 2022

Accepted: 17 September 2022

**Key words:**





Energy balance; glacier mass balance; mass-balance reconstruction; mountain glaciers

**Author for correspondence:**

Tika Ram Gurung,

E-mail: [tikarg@gmail.com](mailto:tikarg@gmail.com)

# A long-term mass-balance reconstruction (1974–2021) and a decadal in situ mass-balance record (2011–2021) of Rikha Samba Glacier, central Himalaya

Tika Ram Gurung<sup>1,2</sup> , Rijan Bhakta Kayastha<sup>2</sup> , Koji Fujita<sup>3</sup> ,  
Sharad Prasad Joshi<sup>1,4</sup>, Anna Sinisalo<sup>1,4</sup> and James D. Kirkham<sup>1,5,6</sup> 

<sup>1</sup>International Centre for Integrated Mountain Development, GPO Box 3226, Kathmandu, Nepal; <sup>2</sup>Department of Environmental Science and Engineering, Himalayan Cryosphere, Climate and Disaster Research Center, School of Science, Kathmandu University, Dhulikhel, Nepal; <sup>3</sup>Graduate School of Environmental Studies, Nagoya University, Nagoya, Japan; <sup>4</sup>GRID-Arendal, Arendal, Norway; <sup>5</sup>Scott Polar Research Institute, University of Cambridge, Lensfield Road, Cambridge CB2 1ER, UK and <sup>6</sup>British Antarctic Survey, Natural Environment Research Council, High Cross, Madingley Road, Cambridge CB3 0ET, UK

**Abstract**

Despite their importance for regional water resource planning and as indicators of climate change, records of in situ glacier mass balance remain short and spatially sparse in the Himalaya. Here, we present an updated series of in situ mass-balance measurements from Rikha Samba Glacier, Nepal, between 2011 and 2021. The updated in situ mass balance is  $-0.39 \pm 0.32$  m w.e. for this period. We use an energy-mass balance model to extend the annual mass-balance series back to 1974. The model is forced using daily meteorological variables from ERA5-Land reanalysis data that is linearly bias-corrected using observations from an automatic weather station situated near the glacier terminus. The modeled mass balance is consistent with the in situ mass-balance series measured 2011–2021 and with previous glaciological and geodetic estimates. The model results indicate a mass balance of  $-0.56 \pm 0.27$  m w.e.  $a^{-1}$  over the reconstruction period of 1974–2021, which is comparable to the mass losses experienced by other Himalayan glaciers during this time. An assessment of the sensitivity of the glacier mass balance to meteorological forcing suggests that a change in temperature of  $\pm 1$  K has a stronger effect on the calculated mass balance compared to a  $\pm 20\%$  change in either precipitation, or relative humidity, or solar radiation.

**1. Introduction**

To predict the effects of climate change and its consequent alterations to water availability in highly populated Himalayan watersheds, it is important to monitor and understand the dynamics of Himalayan glaciers. When measured over long time periods, trends in glacier mass balance can be used as an indicator of climate change (Azam and others, 2018; Bolch and others, 2019). Obtaining long-term observations of glacier surface mass balance and other meteorological variables is thus essential to understand linkages between observed glacier changes and their governing atmospheric drivers (Kaser and others, 2006). Accordingly, observations from multiple benchmark glaciers in different geographic and climatic regions are needed to better understand the response of glaciers to climate change (e.g. Wagnon and others, 2007; Fujita and Nuimura, 2011; Sunako and others, 2019; Wagnon and others, 2020; Stumm and others, 2021). Although mass-balance studies of Himalayan glaciers have been conducted since the 1970s (Fujii and others, 1976), factors including the remoteness of research sites, harsh weather conditions, financial limitations and time constraints have resulted in discontinuous and spatially non-uniform glacier mass-balance records in this region (Gardner and others, 2013; Azam and others, 2018).

Remote-sensing studies reveal that the geodetic mass balance of glaciers in High Mountain Asia ( $-0.18 \pm 0.04$  m w.e.  $a^{-1}$  from 2000 to 2016; Brun and others, 2017;  $-0.19 \pm 0.03$  m w.e.  $a^{-1}$  in between 2000 and 2018; Shean and others, 2020) is less negative than the global mean for glaciers ( $-0.48 \pm 0.20$  m w.e.  $a^{-1}$  between 2006 and 2016) (Zemp and others, 2019). This offset has mainly been attributed to the slightly positive glacier mass-balance trends experienced in the Karakoram and West Kunlun regions, which are driven by differences in monsoonal and westerly weather patterns (Kääb and others, 2012; Brun and others, 2017; Lin and others, 2017; Sakai and Fujita, 2017; Azam and others, 2018).

In situ measurements demonstrate that glacier mass loss is highly spatially heterogeneous in the Himalaya. For example, an extreme mass loss of  $-0.73$  m w.e. at between 2004 and 2014 was reported from ice core measurements at Naimona'nyi Glacier in the western Himalaya at an elevation of 6000 m a.s.l. (Zhao and others, 2016). In contrast, Mandal and others (2020) found the mass balance of Chhota Shigri Glacier to be less negative between 2002 and 2019 ( $-0.46 \pm 0.40$  m w.e.  $a^{-1}$ ), despite being situated in the western Himalaya region. Wagnon and others (2020) reported that Mera Glacier in the eastern Himalaya lost mass at a moderate

© The Author(s), 2022. Published by Cambridge University Press on behalf of The International Glaciological Society. This is an Open Access article, distributed under the terms of the Creative Commons Attribution licence (<http://creativecommons.org/licenses/by/4.0/>), which permits unrestricted re-use, distribution and reproduction, provided the original article is properly cited.

[cambridge.org/jog](https://www.cambridge.org/jog)



rate ( $-0.41 \text{ m w.e. a}^{-1}$ ) between 2007 and 2019. However, significantly higher mass losses ( $-0.80 \pm 0.28 \text{ m w.e. a}^{-1}$ ) have also been reported from the small plateau-type Yala Glacier in the central Himalaya (Stumm and others, 2021). Continuous mass-balance stake measurements (2007–2015) from four glaciers in the Everest region of the eastern Himalaya reveal that the size, shape, elevation and aspect of the glaciers, as well as local climatic influences, are responsible for the heterogeneity in mass balance observed in the region (Wagnon and others, 2013; Sherpa and others, 2017). This finding is also supported by other studies across the Himalaya (e.g., Fujita and Nuimura, 2011; Sunako and others, 2019).

Glacier mass balance also fluctuates seasonally with meteorological conditions in High Mountain Asia. For example, Fujita and others (2011) showed that fluctuations in annual precipitation and summer air temperatures strongly influenced the annual mass balance of Gregoriev Glacier in the Inner Tien Shan region. Summer temperature and winter precipitation are also the main climatic controls on the mass balance of Chhota Shigri Glacier in the western Himalaya (Azam and others, 2014). However, summer temperature has been shown to play no significant role in determining the mass balance of Trambau Glacier in the eastern Himalaya (Sunako and others, 2019).

A number of studies have tried to reconstruct the long-term mass balance of glaciers in the Himalaya by linking in situ observations with energy-balance and/or temperature-index models (e.g., Fujita and Nuimura, 2011; Azam and others, 2014; Zhao and others, 2016; Sunako and others, 2019). These studies by examining different glaciers situated across the Himalaya have revealed spatially heterogeneous mass-balance trends that can be used to fill critical data gaps and help to recognize the impact of climate change on Himalayan glaciers.

Rikha Samba Glacier, a benchmark glacier situated in the central Himalaya, has one of the longest in situ mass-balance records of all Himalayan glaciers. Its mass balance has been measured intermittently since 1974 (Fujii and others, 1976; Fujita and others, 2001; Fujita and Nuimura, 2011) and has been monitored continuously since 2011 (Stumm and others, 2021). In this study, we first present an update of the in situ mass-balance record between 2017 and 2021. Previous observations extend back until 2017 (Stumm and others, 2021). To bridge gaps in the long-term mass-balance record, we then use a physically based energy-mass balance model which is calibrated using in situ mass-balance measurements to reconstruct the mass balance of Rikha Samba Glacier between 1974 and 2021. Finally, we examine the influence of different meteorological drivers of the glacier mass balance.

## 2. Study area, data and methods

### 2.1 Study area

Rikha Samba Glacier ( $28.82^\circ\text{N}$ ,  $83.49^\circ\text{E}$ ) is a valley-type, debris-free glacier located in the central Himalaya (Fig. 1). This area is situated in an arid region on the leeward side of the mountain range called the Hidden Valley, where high ridges and cliffs constitute challenging barriers to site access (Nakawo and others, 1976; Fujita and Nuimura, 2011). The Hidden Valley is one of the driest regions in Nepal. For example, Fujita and others (2001) found that the region received  $\approx 450 \text{ mm}$  of precipitation between October 1998 and September 1999. In comparison, annual precipitation is typically  $<1000 \text{ mm a}^{-1}$  over Nepal's northwestern mountains but can exceed  $3000 \text{ mm a}^{-1}$  in central Nepal (Ichayanagi and others, 2007).

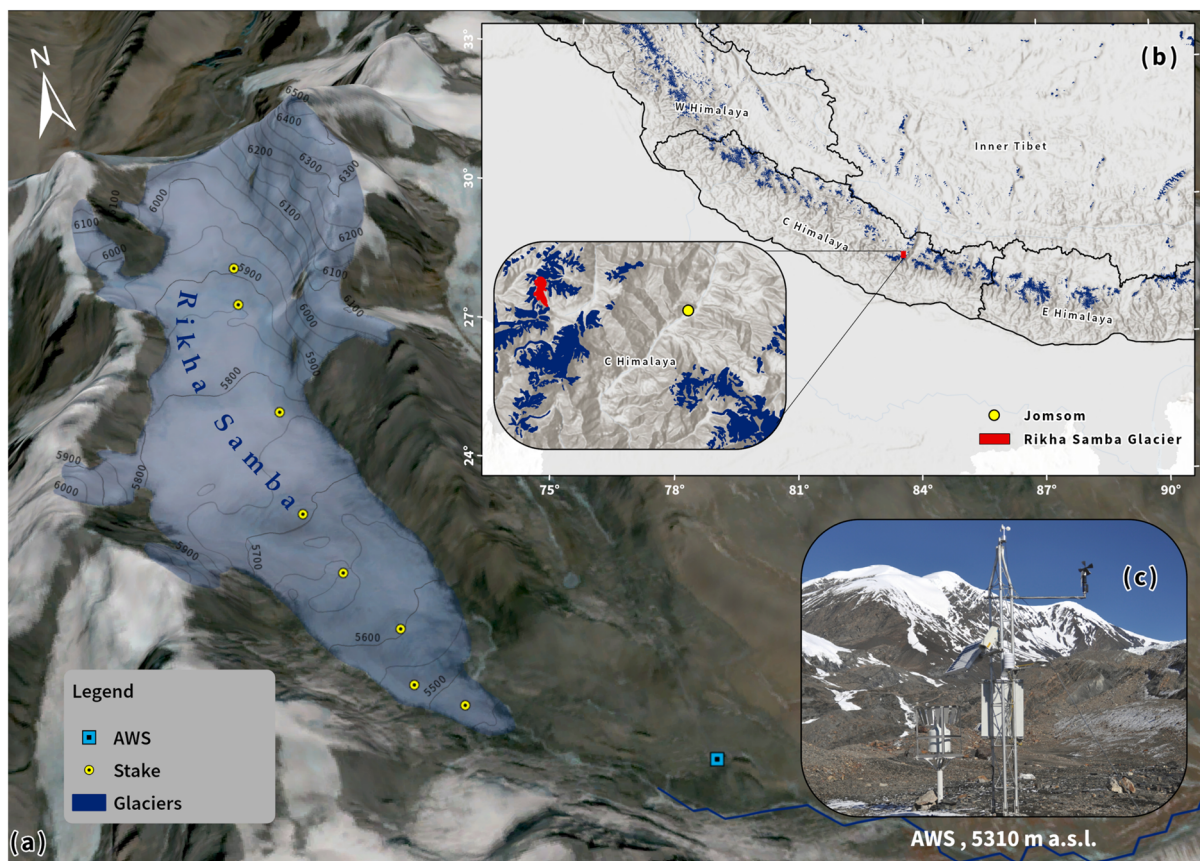


**Fig. 1.** (a, b) Location of Rikha Samba Glacier in the central Himalaya delineated by the Randolph Glacier Inventory version 6.0. (c) Rikha Samba Glacier in relation to the mass-balance stake network (yellow circles) and the off-glacier automatic weather station (AWS; blue square and a photo). Glacier elevation contour lines are displayed from the NASA Shuttle Radar Topography Mission digital elevation model (Zandbergen, 2008) at 50 m intervals.

Rikha Samba Glacier predominantly faces southeast with a mean slope of 13°. As of 2020, the glacier ranges from 5427 to 6515 m a.s.l. with a total length of ~5.5 km and a planimetric area of 5.62 km<sup>2</sup>, which makes it the largest and the longest glacier among the ten glaciers situated in the Hidden Valley (Lama and others, 2015). In previous studies, the glacier area was considered to be 4.81 km<sup>2</sup> (Higuchi, 1977; Fujita and others, 2001) because they did not consider the full extent of the steep accumulation zone of the glacier. Ground-penetrating radar surveys have revealed that the basal regime of Rikha Samba Glacier is polythermal, consisting mostly of cold ice but with temperate ice in the accumulation zone which is strongly influenced by the percolation of meltwater to the bed through crevasse fields (Gilbert and others, 2020). This mechanism is currently driving changes to the glacier's thermal regime at over twice the rate that would be possible through advection-diffusion processes alone (Gilbert and others, 2020).

The first mass-balance measurements of Rikha Samba Glacier were completed in the summer season of 1974 and reported a slightly positive mass balance (Fujii and others, 1976). One-year measurements were also carried out in October 1998 and October 1999 (Fujita and others, 2001). Field-based geodetic mass-balance measurements made using rangefinders or differential GPS were conducted between 1974–1994 and 1998–2010. These measurements revealed that Rikha Samba Glacier experienced an overall mass loss between these study periods (Fujita and others, 1997; Fujita and Nuimura, 2011). Recent observations between 2011 and 2017 also show a negative mass balance of  $-0.39 \pm 0.32$  m w.e. a<sup>-1</sup> (Stumm and others, 2021). Temperature and precipitation measurements in the region record monsoonal weather patterns (Shrestha and others, 1976). The region receives high wind speeds ( $>4$  m s<sup>-1</sup>) during the winter and pre-monsoon seasons, with prevailing northwesterly and southerly wind directions (Shea and others, 2015; Gurung and others, 2016). The long-term precipitation and temperature records from the nearby Jomsom area show that this region has undergone increases in average precipitation at a rate of  $+0.57$  mm a<sup>-1</sup> from 1957 to 2012, and increases in average air temperature at a rate of  $+0.023$ °C a<sup>-1</sup> between 1980 and 2012 (Gurung and others, 2016). However, these trends are not statistically significant at the 95% confidence interval (Gurung and others, 2016).

## 2.2 Observations and data

### 2.2.1 Meteorological data

An automatic weather station (AWS) was mounted near the Rikha Samba Glacier terminus at 5310 m a.s.l., and has been functioning since 2011 (Shea and others, 2015; Gurung and others, 2016). The AWS measures wind speed and wind direction, relative humidity, shortwave radiation, air temperature and precipitation at 15 min intervals (Table 1). Propylene glycol antifreeze was added to the pluviometer to avoid precipitation refreezing inside the instrument. The precipitation recorded by the pluviometer, which does not have a windshield, is affected by precipitation undercatch – the underestimation of precipitation caused by the deflection of

dropping hydrometeors away from the inlet of the pluviometer (Sevruk and others, 1991; Rasmussen and others, 2012; Mekonnen and others, 2015). If uncorrected, this effect can result in an underestimation of precipitation by up to 10% for rainfall and  $>50\%$  for snowfall (Ye and others, 2004; Wolff and others, 2015; Kirkham and others, 2019). The quantity of precipitation recorded by the pluviometer was adjusted for undercatch using the correction function from Kochendorfer and others (2017), which has been shown to perform relatively well for Himalayan environments (Kirkham and others, 2019). The catch efficiency ratio,  $C_E$  of the precipitation gauge is calculated from the correlation function, which uses mean air temperature  $T_{\text{air}}$  (°C), wind speed  $U$  (m s<sup>-1</sup>) and three empirically derived constants (a, b and c), which vary according to the presence or lack of a windshield:

$$C_E = e^{-a(U)(1 - \tan^{-1}(b(T_{\text{air}})+c))}. \quad (1)$$

Wind speeds were downscaled from the height of the anemometer to the lower height of the pluviometer orifice using a logarithmic wind profile (Yang and others, 1998), accounting for relative changes in gauge height due to snow accumulation. The theoretical catch efficiency of the pluviometer for the typical wind speeds and air temperature conditions recorded at the Rikha Samba Glacier AWS was found to be  $57 \pm 26\%$  ( $1\sigma$ ), which agrees well with previous studies (Ye and others, 2004; Wolff and others, 2015). Wind-induced undercatch can therefore result in measurement losses exceeding 50% for solid precipitation at this site.

### 2.2.2 Reanalysis data

Daily ERA5-Land reanalysis (ERA5L) data, including temperature, precipitation, solar radiation, relative humidity and wind speed at surface level (Muñoz-Sabater and others, 2021), were used to calculate glacier mass balance from 1974 to 2021. Wind speed at a 2 m height from the surface ( $U$ ) is calculated from wind speed at a height of 10 m in the reanalysis data ( $U_{10}$ ), based on the assumption of a logarithmic wind profile (Fujita and Sakai, 2014) as described in Eqn (2):

$$U = U_{10} \left[ \frac{\ln\left(\frac{2}{z_0}\right)}{\ln\left(\frac{10}{z_0}\right)} \right], \quad (2)$$

where the surface roughness length ( $z_0$ ) is assumed to be 0.1 m (Fujita and Sakai, 2014).

### 2.2.3 Observed and gap-filled meteorological data

The AWS has recorded relative humidity, air temperature, solar radiation, precipitation and the wind speed at the terminus of Rikha Samba Glacier since September 2011 with occasional data gaps due to battery failures. To fill the missing input data for the energy-mass balance model, variables from the ERA5L dataset

**Table 1.** Overview of AWS and rain gauge instruments and their specifications

Sensor	Parameter	Height above ground (m)	Missing data (% of timeseries)	Accuracy
Rotronic SC2	Air temperature	2.0	26.0	$\pm 0.1$ K
	Relative humidity	2.0	26.0	$\pm 0.5\%$
RM Young 05103-45 Wind Monitor-Alpine Model	Wind direction	3.0	–	$\pm 3.0^\circ$
	Wind speed	3.0	23.0	$\pm 0.3$ m s <sup>-1</sup>
Kipp & Zonen CMP6	Solar radiation	2.8	46.0	$\pm 5.0\%$ for daily totals
Weighing Rain gauge OTT Pluvio2	Precipitation	1.0	34.0	$\pm 0.1$ mm



**Table 2.** Parameters used to adjust the daily meteorological variables at the Rikha Samba Glacier AWS

Variable	<i>m</i>	<i>c</i>	<i>r</i>	<i>p</i> <
Precipitation (mm)	0.24	0	0.47	0.01
Air temperature (°C)	0.67	1.52	0.90	0.01
Solar radiation (W m <sup>-2</sup> )	0.94	36	0.72	0.01
Relative humidity	1.03	-0.23	0.81	0.01
Wind speed (m s <sup>-1</sup> )	3.4	2.94	0.45	0.01

Linear regression ( $y = mx + c$ ) was used to adjust the variables from the ERA5L data ( $x$ ). Also listed are the correlation coefficients ( $r$ ) and the level of significance at the 95 % confidence level ( $p$ ). The regression equation for precipitation was obtained by the assuming a zero intercept ( $c = 0$ ).

were bias-corrected with the AWS data using linear regression (Table 2). Daily minimum values of each variable measured by the AWS are always higher than the ERA5L data, except in the case of air temperature. Table 2 summarizes the correlation coefficients and the regression parameters between the observed AWS data and the ERA5L data for the period from October 2011 to September 2015. The data exhibit statistically significant correlations for all input meteorological variables and the scatter plots between different variables are presented in the Supplementary Information (Fig. S1). Once correlation was established, the model input data were prepared by filling data gaps with the estimated data for four observation years from October 2011 to September 2015 (Fig. 2). These variables were used as inputs for the mass-balance calculations.

Daily temperature lapse rates were applied based on the lapse rates observed in the central Himalayan Langtang catchment (Immerzeel and others, 2014). The Hidden Valley does not have sufficient weather stations to calculate the lapse rate using the same methods as used for other more data-rich areas of the Himalaya (Immerzeel and others, 2014; Thayyen and Dimri, 2018). However, similar temperature and solar radiation patterns

are observed in both the Hidden Valley and the Langtang catchment (Shea and others, 2015).

#### 2.2.4 Mass balance

The mass-balance monitoring program at Rikha Samba Glacier was re-established in 2011 (Gurung and others, 2016; Gilbert and others, 2020; Stumm and others, 2021) after occasional measurements by Japanese research teams in 1974, 1994, 1998, 1999 and 2010 (Fujii and others, 1976, 1997, 2001; Fujita and Nuimura, 2011). Since September 2011, mass-balance observations have been conducted using bamboo stakes (Fig. 1) and snow-pit measurements if snow is present. Harsh weather conditions in 2011 and deep snow deposited by Cyclone Hudhud in 2014 made it difficult to access the upper reaches of the glacier in these years. Deep snow also prevented field teams from entering the Hidden Valley through the ‘high-pass’ in 2020 as the field campaign was started 2 months later than usual because of the travel restrictions imposed due to the COVID-19 pandemic. Consequently, no mass-balance data could be collected in 2020.

Mass balance,  $b_o$  (m w.e.), at a certain stake/point was calculated using changes in stake height, snow thickness and snow and ice densities as:

$$b_o = \Delta S \rho_s + \Delta I \rho_i, \quad (3)$$

where  $\Delta S$  and  $\Delta I$  are the changes in snow thickness (m) and ice level (m), respectively.  $\rho_s$  is snow density (302–575 kg m<sup>-3</sup>) at each snow pit, and  $\rho_i$  is the assumed density of ice (900 kg m<sup>-3</sup>; Stumm and others, 2021).

The glacier-wide mass balance,  $B_a$  (m w.e.), was calculated as:

$$B_a = \frac{\sum_{i=1}^n b_i s_i}{S}, \quad (4)$$

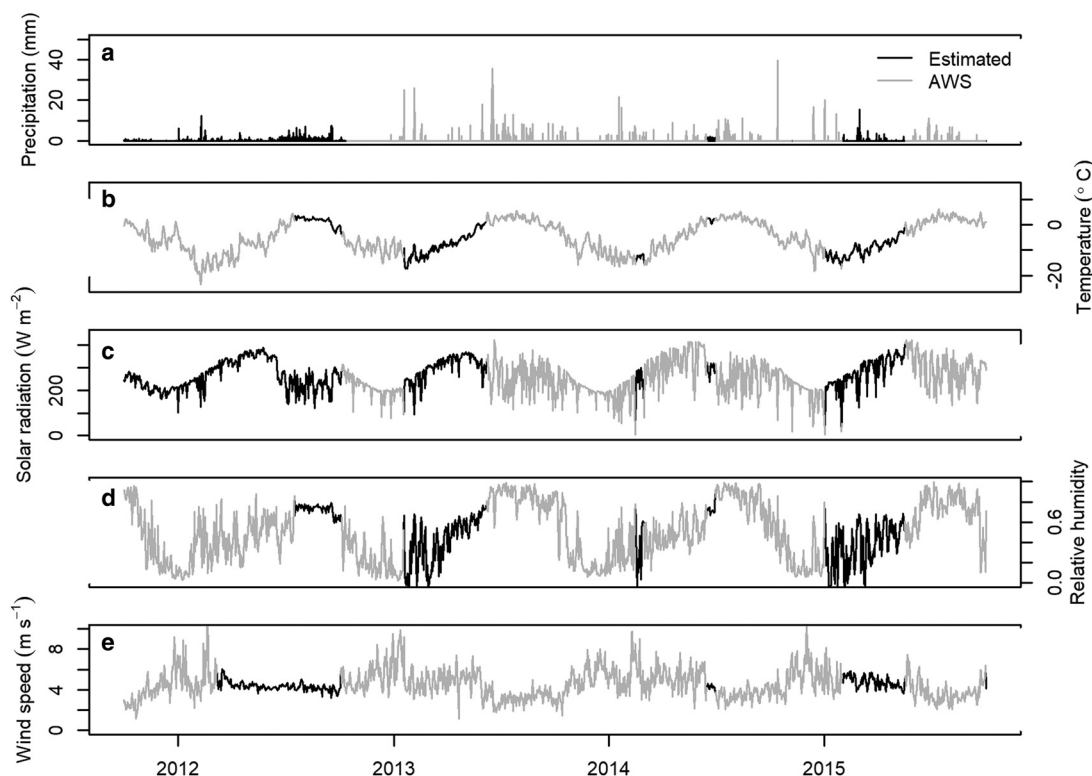


**Fig. 2.** Meteorological observations gathered by the automatic weather station (AWS) from October 2011 to September 2015. Panels (a) to (e) display daily values of precipitation, incoming shortwave radiation, air temperature, relative humidity and the wind speed, respectively. Grey lines and black lines indicate the observed AWS data and the estimated data, respectively. The estimated data are based on the linear relations presented in Table 2.

where  $s_i$  and  $S$  are the area inside a 50 m altitudinal band ( $\text{m}^2$ ) and the total surface area ( $\text{m}^2$ ) of the glacier, respectively.  $b_i$  is the mass balance at each 50 m altitudinal interval; this was derived by linear interpolation of the stake mass balance (Fountain and Vecchia, 1999). The equilibrium-line altitude (ELA) was calculated based on the interpolated mass-balance gradients derived from the point measurements (Stumm and others, 2021). The hypsometry of Rikha Samba Glacier was extracted from the NASA Shuttle Radar Topography Mission digital elevation model (Zandbergen, 2008) using glacier outlines delineated by Landsat satellite images in 1980, 1990, 2000, 2010 and 2020.

We updated the mass-balance record of Rikha Samba Glacier from an earlier study (Stumm and others, 2021) by presenting data gathered during the 2017/18, 2018/19, 2019/20 and 2020/21 field seasons. As the glacier could not be accessed in 2020, the mass balance for the period of 2019–21 was divided by two to estimate the annual mass balance for the 2019/20 and the 2020/21 seasons.

We used mass-balance data from 2011 to 2021 to calibrate the energy-mass balance model described in Section 2.3. Two distinct mass-balance gradients were observed, characterized by a large gradient in the lower ablation zone and a medium gradient in the transition between the ablation and accumulation zones. Point mass-balance measurements below (above) 5650 m a.s.l. were used to derive the mass-balance gradient over the ablation (accumulation) area.

The uncertainty associated with using point mass-balance measurements was calculated by assessing the random errors accumulated by gathering the stake-height measurements. The point measurement error and the error associated with the interpolation methods chosen were applied for the glacier-wide mass-balance uncertainty (Stumm and others, 2021). The uncertainty of the ELA was estimated by shifting the regression lines of the error range of point measurements as described by Stumm and others (2021).

## 2.3 Energy-mass balance model

### 2.3.1 Description of the model

The daily point mass balance of Rikha Samba Glacier at every 50 m elevation interval was calculated using an energy-mass balance model (Fujita and Ageta, 2000; Fujita and others, 2007, 2011). Previously, this model had successfully estimated glacier mass balance, accumulation area ratio (AAR), ELA and runoff for numerous Asian glaciers (Sakai and others, 2009; Fujita and Nuimura, 2011; Zhang and others, 2013; Fujita and Sakai, 2014; Sunako and others, 2019). The model does not take the aspect or the slope of the glacier into account. The daily sum of precipitation and the daily mean values of air temperature, relative humidity, solar radiation and wind speed are the input variables for the model. It is assumed that the input relative humidity, solar radiation and wind speed are independent of altitude. The energy balance at the glacier surface can be stated as:

$$\max[Q_M, 0] = (1 - \alpha) S_{\text{in}} + L_{\text{in}} - \sigma \epsilon_s (T_s^4) + H_s + H_L + Q_G, \quad (5)$$

where  $Q_M$  is the heat for snow/ice melting ( $\text{W m}^{-2}$ ). The first three right-hand side components of Eqn (5) represent the radiative flux, where  $S_{\text{in}}$  is incoming solar radiation,  $T_s$  is the surface temperature ( $^{\circ}\text{C}$ ) and  $\alpha$  is the albedo of the ice or the snow surface. Incoming long-wave radiation ( $L_{\text{in}}$ ) is calculated using an empirical scheme with relative humidity, air temperature and the ratio of shortwave radiation at the surface to that at the top of the atmosphere (Fujita and Ageta, 2000; Fujita and others,

2011). The Stefan–Boltzmann law is used to calculate the outgoing long-wave radiation supposing a black body for the ice/snow surface from modeled surface temperature in Kelvin ( $T_s$ ).  $\sigma$  is the Stefan–Boltzmann constant ( $5.67 \times 10^{-8} \text{ W m}^{-2} \text{ K}^{-4}$ ), and  $\epsilon_s$  is surface emissivity – which is assumed to be 1.0. Snow-surface albedo on a given day was calculated by assuming an exponential reduction of snow albedo toward a given ice albedo with time after a fresh snowfall, as described by Fujita and Sakai (2014). The surface albedo was calculated following Fujita and Sakai (2014), and depends on the amount of snowfall, the air temperature, the number of days after the snowfall and the minimum albedo of the glacier ice, which is expected to be 0.2 (Fujita and Sakai, 2014).

The turbulent sensible ( $H_s$ ) and latent heat ( $H_L$ ) fluxes are calculated using the bulk aerodynamic method as follows:

$$H_s = c_a \rho_a C U (T_a - T_s), \quad (6)$$

$$H_L = l_e \rho_a C U [rhq(T_a) - q(T_s)], \quad (7)$$

where  $c_a$  is the specific heat capacity of air ( $1006 \text{ J kg}^{-1} \text{ K}^{-1}$ ),  $\rho_a$  is air density ( $\text{kg m}^{-3}$ ),  $U$  is wind speed ( $\text{m s}^{-1}$ ),  $l_e$  is the latent heat of evaporation ( $2.50 \times 10^6 \text{ J kg}^{-1}$ ) and  $rh$  is relative humidity. Constant bulk exchange coefficients ( $C = 0.002$ ) (Kondo and Yamazaki, 1986) are used as suggested by Fujita and Ageta (2000). Saturated specific humidity ( $q$ ) is calculated as a function of air temperature ( $T_a$ ) in the model. The surface temperature ( $T_s$ ) is obtained by satisfying Eqn (5) using all of the components (Fujita and Ageta, 2000).  $Q_G$  is sub-surface heat flux. All components are positive when fluxes are directed toward the surface and negative when directed away from the surface.

Most of the precipitation ( $P_p$ ) falls during the monsoon season in the Himalaya (Immerzeel and others, 2014; Shea and others, 2015). Precipitation at high elevations can occur as solid (snowfall), liquid (rainfall) and mixed phases (Kayastha and others, 1999). It is considered that the possibility of snowfall ( $P_s$ ) or rainfall ( $P_r$ ) depends on the air temperature ( $T_a$ ) (Ueno and others, 1994; Sakai and others, 2006) and affects the mass balance of glacier. This is calculated as:

$$P_s = P_p \quad [T_a \leq 0^{\circ}\text{C}],$$

$$P_s = \left(1 - \frac{T_a}{3}\right) P_p \quad [0^{\circ}\text{C} < T_a < 3^{\circ}\text{C}],$$

$$P_s = 0 \quad [T_a \geq 3^{\circ}\text{C}],$$

$$P_r = P_p - P_s.$$

In this model, the mass balance ( $b_m$ ) at any altitudinal point of the glacier is calculated as follows:

$$b_m = P_s - \frac{Q_M}{l_m} - S + R_f. \quad (8)$$

Mass is removed from the glacier as meltwater ( $Q_M/l_m$ ) and sublimation ( $S$ ). Some of the meltwater is retained within the glacier through refreezing ( $R_f$ ).  $l_m$  is the latent heat for melting ice ( $3.33 \times 10^5 \text{ J kg}^{-1}$ ). The extent of meltwater refreezing in the snow layer ( $R_f$ ) is obtained from the change in the vertical ice temperature profile when surface water is present. Further details

about these processes can be found in Fujita and Ageta (2000). Their model solves the energy balance and heat conduction in the glacier and calculates the quantity of refrozen water. The amount of refrozen water within the snow is calculated based on snow temperature changes (Fujita and Ageta, 2000).

### 2.3.2 Calibration and validation of the model

Precipitation lapse rate and precipitation ratio were optimized to obtain a good agreement between the observed and modeled mass-balance profiles. The precipitation ratio refers to the change in the original precipitation value with a certain factor (%). Field-based glacier mass-balance profiles from 1998/99 (Fujita and others, 2001), 2012/13, 2015/16, 2016/17 (Stumm and others, 2021), 2017/18 and 2018/19 (this study) were used to calibrate the model for the reconstruction of mass balance. These profiles were chosen because only these mass-balance years have point mass-balance data from both the ablation and the accumulation zones, despite the regular measurement program having started in 2011. The mass-balance measurements from 2019/20 and 2020/21 were not included in the calibration since these data are averaged from 2019 to 2021. The model was validated by calculating the glacier-wide mass balance and comparing this to the mass-balance years of 2011/12, 2013/14, 2014/15, 2019/20 and

2020/21 which were not used to calibrate the model. Moreover, the point-to-point mass balance at each stake location was also calculated.

### 2.3.3 Sensitivity analysis

The sensitivity of the estimated mass balance was calculated by altering the variables and the parameters used in the model individually while the others remained constant. For instance, the precipitation, solar radiation and the relative humidity used in the model were perturbed by  $\pm 20\%$ , and air temperature by  $\pm 1$  K. Similarly, the mass balance was also calculated by changing the minimum value of the glacier surface albedo ( $\alpha$ ) from 0.2 to 0.4, and 0.2 to 0.0. The critical temperature ( $CT_a$ ) to separate snow and rain was also altered between 1 and  $5^\circ\text{C}$ .

## 3. Results

### 3.1 Observed mass balance and related variables

The point mass balances as a function of elevation for each observational year using linear regression are shown in Figure 3 (updated from Stumm and others (2021) with the new mass-balance data from 2017 to 2021). Similarly, glacier-wide mass balance ( $B_a$ ), ELA, AAR and the glacier mass-balance gradients are

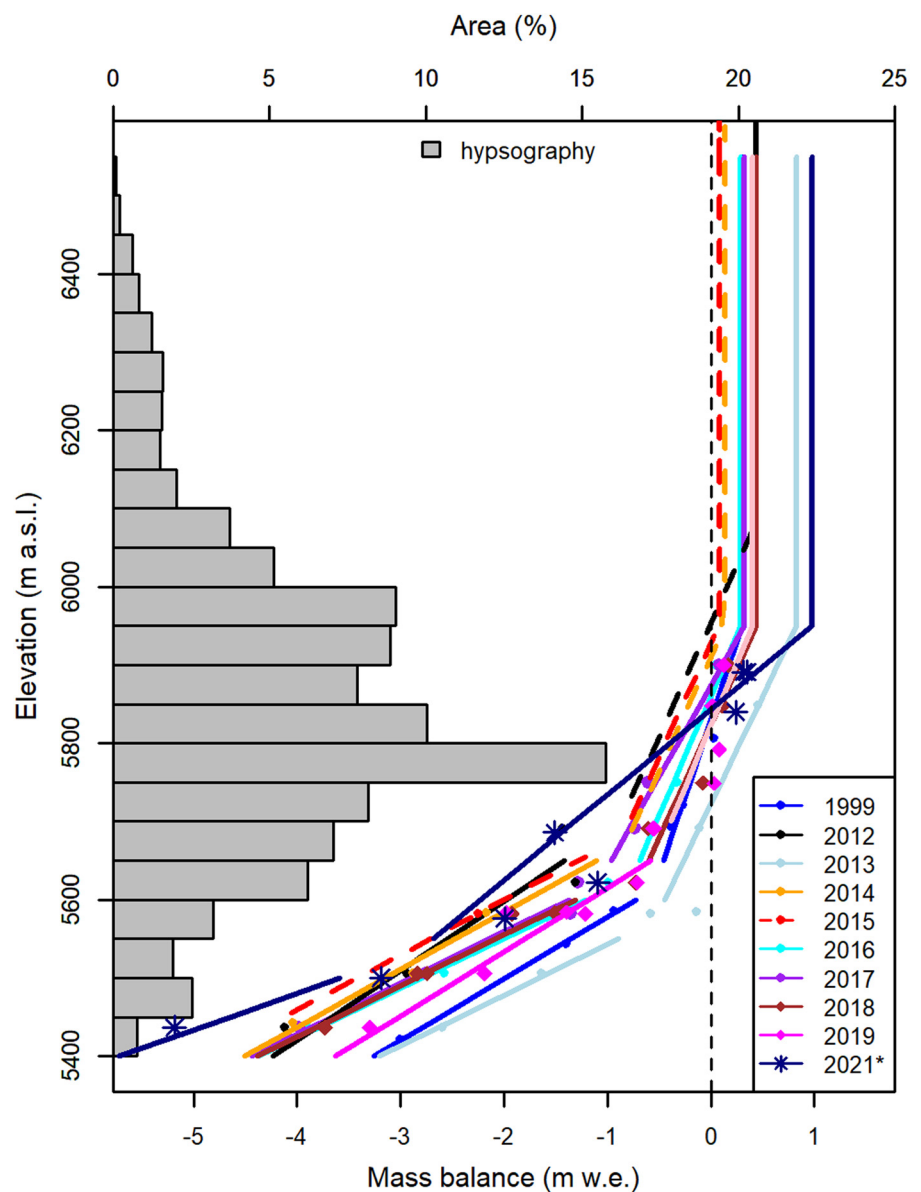


**Fig. 3.** Hypsometry and observed mass-balance profiles of Rikha Samba Glacier. The hypsometry of the glacier (grey bars) is shown at 50 m elevation intervals. The stake mass balance and its linear regression lines as a function of elevation are shown from the mass-balance years of 1998/99 (Fujita and others, 2001), 2011–2017 (Stumm and others, 2021), 2017/18, 2018/19 and 2019/21. The year 2021\* refers to the 2-year mass-balance measurement from 2019 to 2021.

presented in Table 3. The altitudinal mass-balance profiles of 2017/18, 2018/19, 2019/20 and 2020/21 have similar patterns to previous observational years; glacier-wide mass balance is negative (Stumm and others, 2021). The years of 2017/18 and 2018/19 had mass balances of  $-0.38 \pm 0.26$  and  $-0.26 \pm 0.32$  m w.e., respectively. In comparison, the annual mass balance for the years between 2019 and 2021 was  $-0.27 \pm 0.36$  m w.e.  $a^{-1}$  when averaged over the 2-year period. Averaged annual  $B_a$  and cumulative  $B_a$  were  $-0.39 \pm 0.32$  and  $-3.52$  m w.e.  $a^{-1}$ , respectively, for the one-decade period from 2011 to 2021 (Table 3). All observational years have a negative mass balance except in 2013 (+0.12 m w.e.). Rikha Samba Glacier experienced strong interannual variability in mass balance between 2011 and 2021, fluctuating from the most negative mass-balance year in 2011/12 ( $-0.72$  m w.e.) to a positive mass-balance year in 2012/13 (+0.12 m w.e.), followed by a less negative mass-balance year in 2014/15 ( $-0.63$  m w.e.) (Stumm and others, 2021).

The vertical gradients of annual mass balance in 2017/18 and 2018/19 for the lower and higher regions of the glacier also vary within the range of previous observations (Table 3). The two-year mass-balance gradient from 2019 to 2021 is quite steep compared to the annual values of the other years presented in Table 3. The mean glacier mass-balance gradient is much greater in the lower area of the glacier (5415– $\approx$ 5800 m a.s.l.) compared to the higher portion of the glacier ( $\approx$ 5800–5950 m a.s.l.), with a mean value and std dev. of  $1.54 \pm 0.32$  m w.e.  $(100 \text{ m})^{-1}$  and  $0.46 \pm 0.23$  m w.e.  $(100 \text{ m})^{-1}$ , respectively. However, because of the incomplete mass-balance measurements in the upper region of the glacier in 2011 and 2014, the  $B_a$  calculation for the mass-balance years of 2011/12, 2013/14 and 2014/15 is based on the mean mass-balance gradient of other mass-balance years including 1998/99 (Fujita and others, 2001). Accordingly, the  $B_a$ , ELA and AAR may not characterize the true picture of the glacier health for those mass-balance years. Hence, ELA and AAR of these years are not discussed further here.

The highest ELA was observed in the year of 2015/16 at an elevation of 5870 m a.s.l., followed by the less negative mass-balance year of 2016/17 (5860 m a.s.l.). The lowest ELA was observed in 2013 (5725 m a.s.l.). The mean ELA between 2011 and 2021, excluding incomplete mass-balance measurement years, was 5829 m a.s.l. with a std dev. of  $\pm 54$  m. Similarly, the highest AAR was 0.76 in 2012/13, while the lowest AAR occurred in 2016/17 with a value of 0.4. The mean AAR during the observational period is  $0.49 \pm 0.14$ .

### 3.2 Calibration of the energy-mass balance model

To calibrate the energy-mass balance model, mass-balance calculations were performed using the gap-filled meteorological data

for the mass-balance years of 1998/99, 2012/13, 2015/16, 2016/17, 2017/18 and 2018/19. A one-year timeseries for the model is run from 01 October to 30 September of the following year. The precipitation gradient is unknown due to a lack of spatial observations and has stronger vertical dependence compared to other meteorological variables in mountainous regions (Immerzeel and others, 2014; Sakai and others, 2015; Soheb and others, 2020). The energy-mass balance model is sensitive to surface albedo (Fujita, 2008; Johnson and Rupper, 2020; Srivastava and Azam, 2022), as well as the critical temperature for separating snow and rain (Srivastava and Azam, 2022); these uncertainties are assessed in the sensitivity analysis (Section 4.2).

To account for uncertainties related to the precipitation gradient, we investigated the best set of precipitation ratios relative to the estimated precipitation and the elevation gradient of precipitation to yield the best estimate mass-balance profiles for the calibration years. To achieve this, we calculated the root mean square error (RMSE) among the observed and modeled mass-balance profiles during the calibration years (Fig. 4). Based on previous studies in the Himalaya (Immerzeel and others, 2014; Sakai and others, 2015), and the lowest RMSE, we adopted a  $-15$  to  $15\%$   $\text{km}^{-1}$  elevation precipitation gradient and a 94–124% precipitation ratio guided by the undercatch predicted to occur in this setting (Section 2.2.1). This is shown by the square box in Figure 4. Values within the boundary of this square box are used for the subsequent calculation of the mass balance of Rikha Samba Glacier.

Observed and modeled mass-balance profiles for the observational years are shown in Figure 5. The grey lines (based on 961 model runs) enclose the modeled mass balance produced by changing the set of precipitation ratios (94–124%) with a 1% increment against the estimated precipitation at the AWS location and the elevation gradient of precipitation with sequential order from  $-15$  to  $15\%$  per km. The red dots with error bars show the observed mass-balance profiles (Figs 5a–k). The modeled mass-balance profiles didn't match well with the observed mass balance for the years 2011/12 and 2013/14 (Figs 5b, d) – particularly in the lower portion of the glacier (5427–5500 m a.s.l.). These patterns are also visible in the scatter plot (Fig. 5l). This tendency may be explained by annual variations in precipitation fall timing and other climatic variables (Sunako and others, 2019; Zhu and others, 2021). However, the overall agreement between the in situ measurements and the model calculations suggests that the energy-mass balance model is robust enough to estimate the former mass balance of Rikha Samba Glacier.

### 3.3 Mass-balance reconstruction

The historical mass balance of Rikha Samba Glacier, reconstructed over 47 years between 1974 and 2021, is displayed in

**Table 3.** Updated surface mass balance ( $B_a$ ), equilibrium line altitude (ELA), area accumulation ratio (AAR) and the mass-balance gradients ( $db/dz$ ) of Rikha Samba Glacier

Mass-balance year	$B_a$ (m w.e.)	ELA (m a.s.l.)	AAR	$db/dz_{\text{low}}$ (m w.e. $100 \text{ m}^{-1}$ )	$db/dz_{\text{high}}$ (m w.e. $100 \text{ m}^{-1}$ )
1974 July–August	0.23 (summer)	–	–	–	–
1998/99	$-0.18$	$5790 \pm 50$	0.49	1.27	0.25
2011/12	$-0.72 \pm 0.34$	–	–	1.13	–
2012/13	$0.12 \pm 0.32$	$5724 \pm 20$	0.75	1.57	0.37
2013/14	$-0.55 \pm 0.34$	–	–	1.36	–
2014/15	$-0.63 \pm 0.35$	–	–	1.48	–
2015/16	$-0.33 \pm 0.27$	$5872 \pm 50$	0.41	1.64	0.36
2016/17	$-0.23 \pm 0.31$	$5862 \pm 50$	0.54	1.89	0.46
2017/18	$-0.38 \pm 0.26$	$5850 \pm 40$	0.37	1.60	0.35
2018/19	$-0.26 \pm 0.32$	$5823 \pm 30$	0.44	1.22	0.31
2019/21	$-0.54 \pm 0.36$	$5844 \pm 30$	0.45	2.14	0.91
Mean	$-0.39 \pm 0.32$	5829	0.49	1.54	0.46
SD	0.26	54	0.14	0.32	0.23



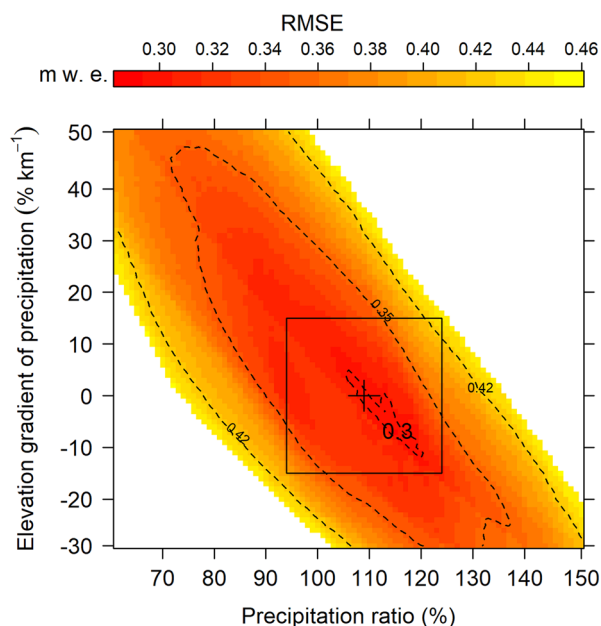


**Fig. 4.** Root mean square error (RMSE) of the model performance for Rikha Samba Glacier. RMSE was calculated between the observed mass-balance years of 1998/99, 2012/13, 2015/16, 2016/17, 2017/18 and 2018/19, and the modeled mass balance as a function of the precipitation ratio (horizontal axis) against the estimated precipitation at the AWS location and the elevation gradient of precipitation (vertical axis) for the same period. The '+' sign in the inset box indicates the smallest RMSE.

**Figure 6.** Five different glacier boundaries from 1980, 1990, 2000, 2010 and 2020 were used to calculate the glacier-wide mass balance. The 1980 glacier boundary was used to calculate the mass balance from 1974–1985, and the 1990 glacier boundary for 1985–1995. Similarly, the 1995–2005 and 2005–2015 mass-balance calculations used the 2000 and 2010 glacier boundaries, respectively. The 2020 glacier boundary was used to calculate the most recent 6-year mass-balance data from 2015–2021.

The results indicate that Rikha Samba Glacier has been losing mass at an average rate of  $-0.56 \pm 0.27$  m w.e.  $a^{-1}$  throughout the modeled period from 1974–2021. The maximum mass loss ( $-1.2$  m w.e.) was observed in the year of 1976/77, whereas 1974/75 was the most positive mass-balance year (0.1 m w.e.). The average mass-loss rates for the decades of 1974–1985 and 1985–1995 were similar at  $-0.67$  m w.e.  $a^{-1}$ . Similarly, mass balance was negative at an average rate of  $-0.56$  m w.e.  $a^{-1}$  between 1995–2005, and 2005–2015, while a mass loss of  $-0.26$  m w.e.  $a^{-1}$  occurred between 2015 and 2021.

For the mass-balance years of 2011–2021, the modeled  $B_a$  was somewhat less negative than that in the previous decades at  $-0.35$  m w.e.  $a^{-1}$ , which is very close to the in situ observations ( $-0.39$  m w.e.  $a^{-1}$ ) for the same period. A comparison of in situ and modeled  $B_a$  for the observational years of 2011–2021 is also presented in **Figure 6a**. The first mass-balance measurement of Rikha Samba Glacier during the summer season of 1974 (Fujii and others, 1976) is also displayed in **Figure 6a**. However, it should be noted that this measurement is not directly comparable to the annual mass-balance calculation presented here as Fujii and others (1976) only conducted the mass-balance measurement during the months of July and August in 1974.

The annual variability in mass balance during the reconstruction period is statistically significant (Sen's slope of 0.01,  $p < 0.01$ ) whereas the input annual precipitation (Sen's slope of 0.67, insignificant at  $p < 0.01$ ) and the summer air temperature (JJAS; Sen's slope of 0.01, insignificant at  $p < 0.02$ ) do not experience significant changes over the reconstruction period. The overall mass-balance calculations demonstrate that the glacier mass-loss rate

was higher ( $-0.65$  m w.e.  $a^{-1}$ ) prior to 2000 than in recent decades ( $-0.47$  m w.e.  $a^{-1}$ ), as shown in **Figure 6a**. Sunako and others (2019) also suggest that greater glacier mass loss occurred prior to 2000 based on a mass-balance reconstruction of Trambau Glacier in the eastern Himalaya between 1979 and 2018. However, an examination of the energy balance records for the entirety of Rikha Samba Glacier (23-elevation interval points) fails to find a statistically significant difference between the time periods before and after the year 2000. A decrease in the total available energy for melt over the entire glacier after 2000 (Table S2) may explain the less negative mass balance in recent decades.

The mean calculated  $B_a$  for Rikha Samba Glacier between 1974 and 1994 ( $-0.66$  m w.e.  $a^{-1}$ ) compares well with the geodetic mass balance measured between 1974 and 1994 ( $-0.57$  m w.e.  $a^{-1}$ ; Fujita and Nuimura, 2011). Similarly, the geodetic mass balance surveyed by Fujita and Nuimura (2011) was  $-0.48$  m w.e.  $a^{-1}$  between 1998 and 2010; our results estimate a  $B_a$  of  $-0.60$  m w.e.  $a^{-1}$  for the same period. Gilbert and others (2020) found almost the same value for the average mass-balance  $B_a$  ( $-0.53$  m w.e.  $a^{-1}$ ) as in our study ( $-0.60$  m w.e.  $a^{-1}$ ) for the years between 1981 and 2015. The mean ELA for the modeled period (1974–2021) is 5808 m a.s.l., with a std dev. of  $\pm 38$  m a.s.l. This ELA is comparable to the value calculated by Gilbert and others (2020) between 1981 and 2015 ( $5864 \pm 42$  m a.s.l.). Overall, the calculated  $B_a$  and ELA are consistent with observational data and the data from previous geodetic and modeling studies (Fujita and Nuimura, 2011; Gilbert and others, 2020).

The summer mean (June to September) air temperature (JJAS temperature) for the modeled time period is presented in **Figure 6c**. These data indicate that at the location of the AWS, positive temperatures are experienced from June to September with a maximum average temperature in July ( $1.35^\circ\text{C}$ ) based on the estimated temperature data from 1974 to 2021.  $B_a$  variability is correlated more strongly with the annual precipitation than with the mean summer air temperature (**Fig. 6c**). Based on previous studies in the Tien Shan region (Fujita and others, 2011) and the eastern Himalaya (Sunako and others, 2019), the climatic variables responsible for driving contrasting annual glacier mass-balance trends differ in space and with the time of year. The same studies show that the summer air temperature is more dominant than annual precipitation in terms of its effect on glacier mass-balance variability. The distinctive characteristics of different glaciers with the response to climate might be associated with the direct alteration of surface albedo and the accumulation of snow on glaciers due to seasonal precipitation patterns, although this factor differs with glacier type and locality (Fujita, 2008; Yamaguchi and Fujita, 2013).

## 4. Discussion

### 4.1 Spatial characteristics of energy-balance components on mass balance

Boxplots of the mean daily surface energy-balance components of Rikha Samba Glacier in the ablation zone (5450 m a.s.l.) and in the accumulation zone (6000 m a.s.l.), between 01 October 2011 and 30 September 2015, are shown in **Figure 7**. Overall, the mean daily total available energy ( $Q_M$ ) was positive ( $25$   $\text{W m}^{-2}$ ) in the ablation zone and was negative ( $-2$   $\text{W m}^{-2}$ ) in the accumulation zone. The main energy input for both locations is the net shortwave radiation ( $S_{\text{net}}$ ): 125 and 86  $\text{W m}^{-2}$  for the ablation and accumulation zones, respectively. The net longwave radiation energy ( $L_{\text{net}}$ ) constituted a net loss of energy (Litt and others, 2019) of  $\sim -77$   $\text{W m}^{-2}$  in the ablation zone and  $-72$   $\text{W m}^{-2}$  in the accumulation zone. Mean daily sensible turbulent heat ( $H_s$ ) and latent heat ( $H_L$ ) are positive and negative at both the



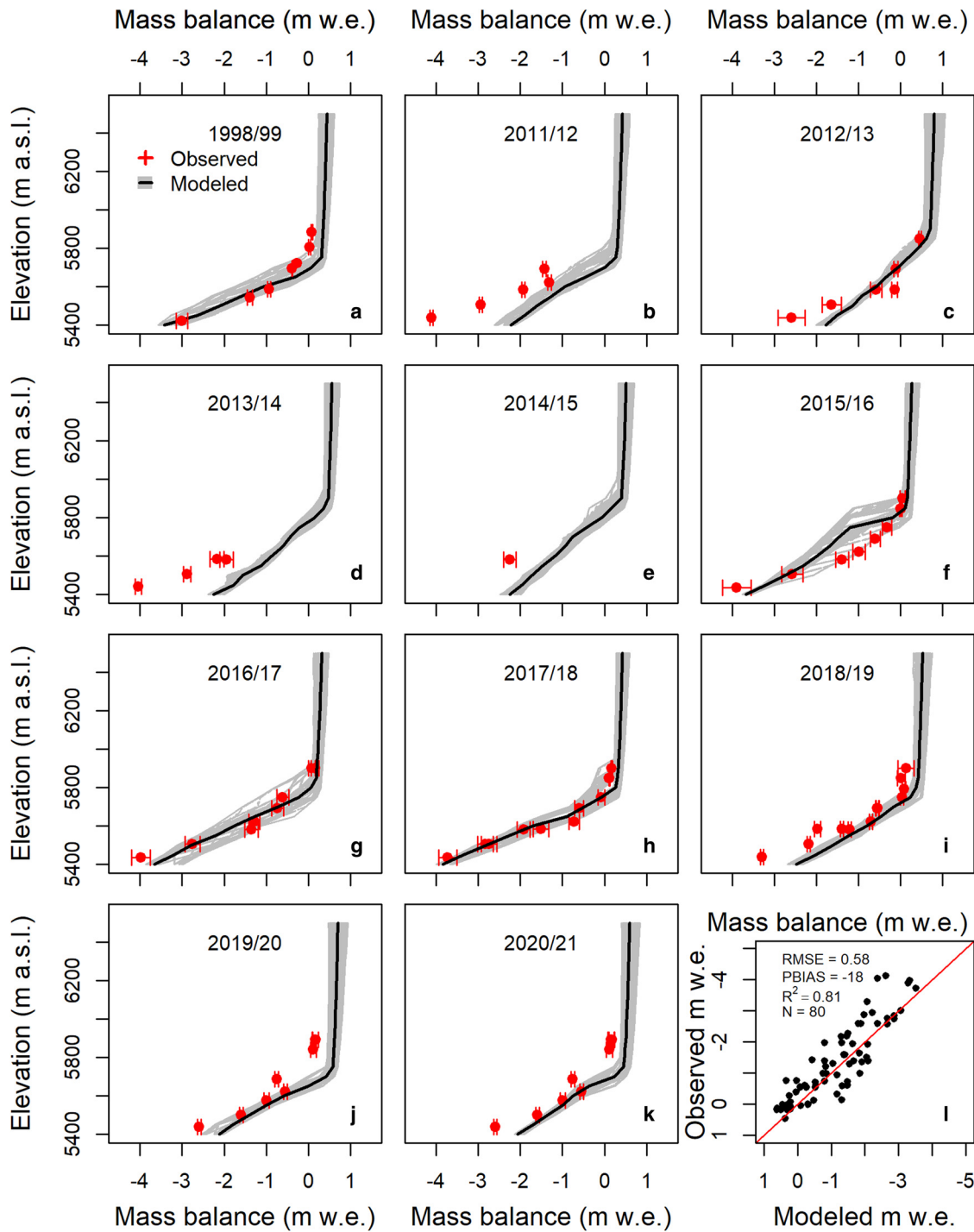


**Fig. 5.** Observed and modeled altitudinal mass-balance profiles of Rikha Samba Glacier for the periods 1998/99 and 2011–2021. Red dots with error bars are the observed mass balance. Black lines with grey shaded regions, which consist of 961 lines, are the modeled mass-balance profiles produced by the method described in Section 3.2. Graph (l) is a scatter plot between the observed and modeled point mass balance, where RMSE refers to the root mean square error and PBIAS is percentage bias.

locations, respectively. On average, a slight energy loss is observed due to the turbulent heat fluxes ( $H_s + H_L$ ) in the ablation ( $-23 \text{ W m}^{-2}$ ) and accumulation zones ( $-16 \text{ W m}^{-2}$ ).

Similarly, the contribution of melt to the glacier mass balance is analyzed as a case study at both locations for same period. The role of melt in point mass balance at the elevation of 5400 m a.s.l. is substantially higher (75%) than at 6000 m a.s.l., which only contributes  $\approx 4\%$ . Sublimation plays a critical role in regulating the mass-balance changes experienced by Himalayan glaciers. A recent study by Potocki and others (2022) found that sublimation drives mass loss even at extremely high elevations such as at Mt.

Everest’s highest glacier (South Col Glacier, 8020 m a.s.l.). Mandal and others (2022) also observed high rates of snow sublimation while analyzing the 11-year meteorological dataset from the lateral moraine of Chhota Shigri Glacier. The role of sublimation in mass balance is higher at 6000 m a.s.l. (26%) than at 5450 m a.s.l. (10%) for Rikha Samba Glacier. The overall loss from sublimation is 22%, which is similar to other Himalayan glaciers (Srivastava and Azam, 2022). Re-sublimation processes also affect the mass-balance trends of Rikha Samba Glacier as we can attribute a 4% and  $\approx 1.5\%$  contribution to positive mass balance in the accumulation and ablation zones, respectively.

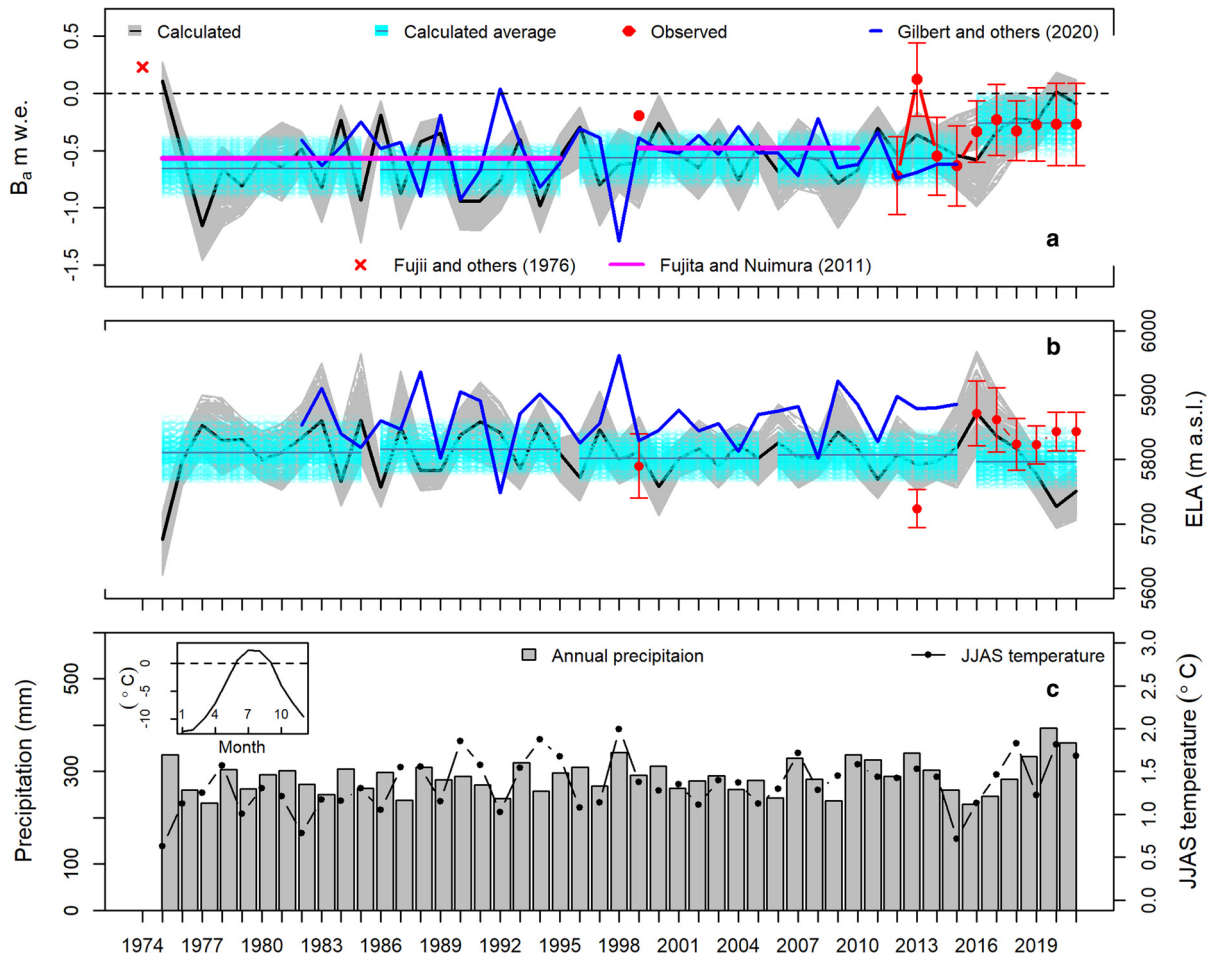


**Fig. 6.** Comparison between the reconstructed mass balance of Rikha Samba Glacier with field-based observations for the period of 1974–2021. (a) Time series of glacier-wide observed, modeled and geodetic surface mass balance. (b) Observed and modeled equilibrium line altitude (ELA). (c) Annual precipitation (bars) and June–September (JJAS) mean air temperature data (dotted line) at the AWS location which were used to force the mass-balance calculation. The inset plot in (c) shows the average monthly mean air temperature data at the AWS location between 1974 and 2021.

#### 4.2 Mass-balance sensitivities

The std dev. for the inter-annual variability of air temperature, precipitation, solar radiation and relative humidity are  $0.64^{\circ}\text{C}$ ,  $50.60\text{ mm}$  (17.88%),  $5.65\text{ W m}^{-2}$  (2.17%) and  $0.02$  (4.10%),

respectively. The sensitivity of the calculated glacier-wide mass balance to different meteorological variables was examined (Fig. 8, Table S3) by altering the value of precipitation, solar radiation and relative humidity by  $\pm 20\%$ , while air temperature was

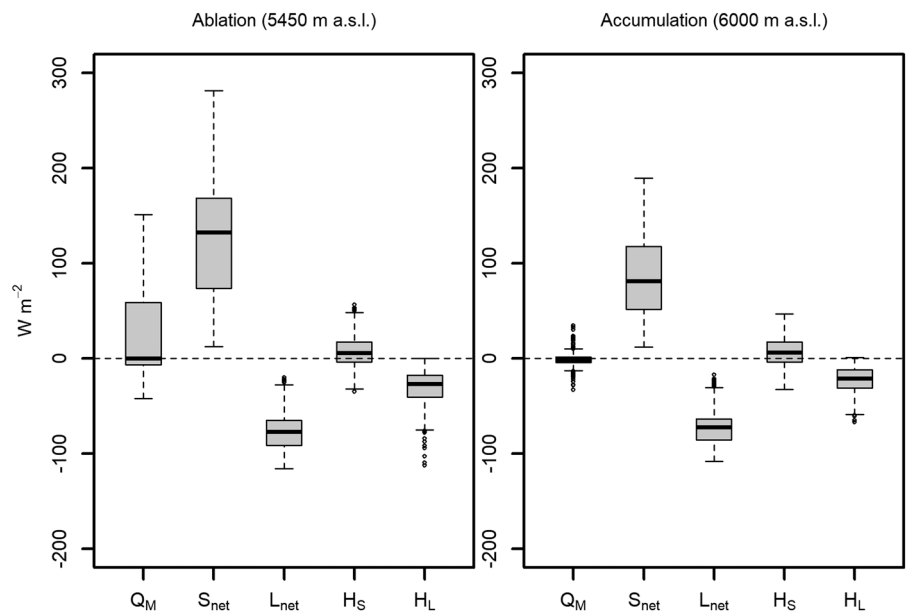


**Fig. 7.** Average daily surface energy-balance components calculated at the ablation and accumulation zones between 01 October 2011 and 30 September 2015. Each boxplot's boundaries show the upper and lower quartiles, while the middle line of the boxplot shows the median value. Whisker ends indicate the maximum and minimum values.

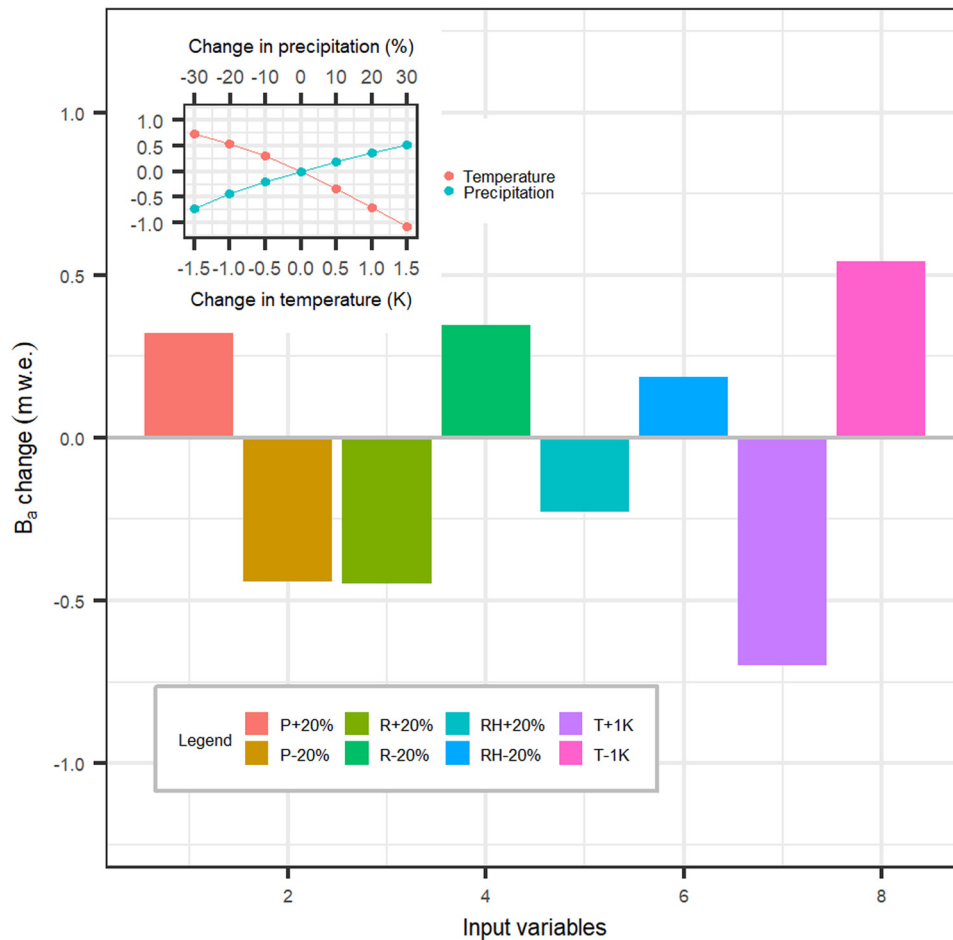


**Fig. 8.** Glacier-wide mass-balance sensitivity to the meteorological variables. Sensitivity was analyzed by changing the quantity of precipitation ( $P \pm 20\%$ ), solar radiation ( $R \pm 20\%$ ), relative humidity ( $RH \pm 20\%$ ) and temperature ( $T \pm 1\text{ K}$ ) forcings in the model. The results indicate that the mass balance is more sensitive to changes in temperature than for other variables. The inset map shows the response of the calculated mass balance to perturbations in air temperature and precipitation by increments of 0.5 K from  $-1.5$  to  $+1.5$  K for temperature, and for increments of 10% between  $-30$  and  $+30\%$  for precipitation.

varied by  $\pm 1\text{ K}$  throughout the modeled period. All other input variables remained unchanged while perturbing the assigned variable. The average mass-balance change over the modeled period reflects its sensitivity to the perturbations. Mass-balance changes of  $0.35\text{ m.w.e. a}^{-1}$  (65%) and  $-0.44\text{ m.w.e. a}^{-1}$  (−80%) can be expected if we increase or decrease precipitation by 20%, respectively. Similarly, altering the magnitude of incoming solar radiation by  $\pm 20\%$  can increase and decrease the modeled mass balance by  $-81$  and  $63\%$ , respectively. In general, precipitation and solar radiation have an almost equal influence on mass balance but in opposing directions. Increasing relative humidity by 20% decreases the calculated mass balance by 41%, while mass balance increases by 34% if relative humidity is reduced by the same proportion.  $B_a$  decreases significantly by  $-0.69\text{ m.w.e. a}^{-1}$  (−127%) when air temperature is increased by 1 K, whereas  $B_a$  increases by  $0.54\text{ m.w.e. a}^{-1}$  (98%) when air temperature is decreased by 1 K.

Air temperature and precipitation are commonly used to understand the climatic sensitivity of glacier mass balance. We further assess the response of the mass balance of Rikha Samba Glacier to precipitation and air temperature by considering six scenarios in which air temperature is altered in 0.5 K intervals between  $-1.5$  and  $+1.5$  K. Similarly, precipitation is varied by 10% at intervals between  $-30$  and  $+30\%$ . The mass balance decreased by  $-194\%$  when air temperature was increased by 1.5 K, whereas the calculated mass balance increased by 133% when air temperature was decreased by the same proportion.

The total mass balance varied by  $\sim \pm 35\%$  when precipitation was varied by  $\pm 10\%$ . Similarly, the calculated mass balance increased and decreased by 94 and  $-133\%$  when precipitation was increased and decreased by 30%, respectively.

Taking into account a positive std dev. of the inter-annual variability of air temperature and precipitation such as  $+0.64^\circ\text{C}$  and  $+50.60\text{ mm}$ , respectively, the corresponding biases for the resulting change in mass balance were  $\approx -0.48$  and  $\approx 0.40\text{ m.w.e.}$ , respectively. Similarly, if we consider a negative std dev., the change in mass balance would be  $\approx 0.35$  and  $\approx -0.40\text{ m.w.e.}$ , respectively (Fig. 8 inset). The inset plot in Figure 8 also suggests that air temperature dominates over precipitation when determining the rate of mass-balance change. Consequently, the negative mass balance reported for Rikha Samba Glacier mostly results from increasing air temperature. This conclusion also supports the results of Che and others (2019) for the Urumqi River Glacier No.1 in the Tian Shan region.

#### 4.3 Mass-balance response to parameters

Surface albedo has a strong effect on glacier melting. If the assumed minimum glacier ice surface albedo is increased from 0.2 to 0.4, the glacier mass balance would become more positive by 57%. Similarly, if we assume an ice surface albedo of 0.1, the mass balance would be 31% more negative (Table S4). However, perturbing the maximum critical temperature to separate snow and rain between 1 and  $5^\circ\text{C}$  from the reference run of  $3^\circ\text{C}$  did



not have a hugely significant impact on the modeled mass balance. If a maximum critical temperature of 1°C is assumed, the mass balance would become more negative by –4%, whereas at 5°C a 10% more positive mass-balance change would have been observed.

Furthermore, the impact of using a constant glacier boundary on mass balance was also assessed. If only the recent 2020 glacier boundary is used to reconstruct the mass balance for the whole modeled period, then the mass balance would become less negative by 14%. Similarly, if the 2000 and 1980 glacier boundaries are used, the mass balance would change by –6 and –13% respectively from the present calculation. This consideration is important, as the terminus of Rikha Samba Glacier has continuously retreated since 1974 (Fujita and others, 2001; Bajracharya and others, 2015; Stumm and others, 2021), reducing the overall glacier area by almost 15% in 40 years between 1980 (6.65 km<sup>2</sup>, Bajracharya and others, 2015) and 2020 (5.62 km<sup>2</sup>).

Due to the limited duration of the meteorological data, which is less than that required to run a full energy-mass balance model, we instead use the bias-corrected ERA5 and ERA5L data at AWS location for the mass-balance calculation. To determine the applicability of these datasets and the validity of the bias-correction method, we conducted multiple case studies, similar to the method described in Section 3.2, to obtain the lowest RMSE values of the modeled and observed mass-balance profiles for the calibration period. Firstly, the linear bias-correction of the input variables were tested on daily (single equation), monthly, four-season and two-season timescales as shown in Table S1 for each ERA5 and ERA5L dataset. Secondly, the model was calibrated using the bias-corrected data. Finally, the use of ERA5L data with the single linear equation bias-correction method was chosen as it is characterized by the smallest RMSE values among the pre-described condition (Table S2).

#### 4.4 Comparison with other studies

The mass-balance reconstruction presented here provides an opportunity to make comparisons with similar studies that employed melt models integrated with field-based studies in the Himalaya. A mass-balance reconstruction of the monsoon-dominated debris-free Trambau Glacier in the eastern Himalaya was found to be –0.65 m w.e. a<sup>–1</sup> between 1979 and 2018 (Sunako and others, 2019), which is more negative than the rate observed at Rikha Samba Glacier. The modeled and observed mass balances of two small glaciers situated to the east of Rikha Samba Glacier – AX010 Glacier (eastern Himalaya) and Yala Glacier (central Himalaya) – exhibit largely negative mass-balance trends (e.g., Kayastha and others, 1999; Acharya and others, 2019) compared to the present study on Rikha Samba Glacier. In addition, a modeling study of Dokriani Glacier from the central Himalaya to the west of Rikha Samba Glacier revealed that this glacier has experienced moderate mass losses with an annual loss of –0.25 ± 0.37 m w.e. a<sup>–1</sup> from 1979 to 2018 (Azam and Srivastava, 2020).

Model results and field observations at Chhota Shigri Glacier (located ≈680 km west of Rikha Samba Glacier in a monsoon-arid transition climate, western Himalaya) demonstrate that this glacier has experienced a moderate mass loss of –0.30 ± 0.36 m w.e. a<sup>–1</sup> between 1969 and 2012 (Azam and others, 2014). A study by Soheb and others (2020) also found that Stok Glacier, a glacier located in the arid western Himalaya, has lost mass at a moderate rate (–0.47 ± 0.35 m w.e. a<sup>–1</sup>) in the 28 years spanning 1978–2019. Naimona'nyi Glacier in the same region has lost mass at a rate of –0.39 m w.e. a<sup>–1</sup> between 2010 and 2018 (Zhu and others, 2021). Another study employing an energy-mass balance model approach to Chhota Shigri Glacier in the western Himalaya and to Dokriani Glacier in the central Himalaya

reported mean glacier-wide mass balances of  $B_a$  –0.31 ± 0.38 and –0.27 ± 0.32 w.e. a<sup>–1</sup>, respectively, between 1979 and 2020 (Srivastava and Azam, 2022).

Comparisons with these studies indicate that the rate of shrinkage of Rikha Samba Glacier is within the observed range of other glaciers in the Himalaya. Greater rates of mass-balance decline are observed for glaciers which are situated further to the east of Rikha Samba Glacier than for those located further to the west. Glaciers in the Himalaya are experiencing heterogeneous mass losses due to contrasting glacier geometries (e.g., elevation difference, orientation, shape and size) and differences in the magnitude and timing of monsoonal precipitation (Fujita and Nuimura, 2011; Yamaguchi and Fujita, 2013; Sherpa and others, 2017).

#### 4.5 Model limitations

Himalayan glaciers exhibit complex dynamics that are simplified in numerical model simulations, so even a small error can have a large effect on the result's confidence (Sauter and Obleitner, 2015). The energy-mass balance model employed in this study works using elevation intervals along the length of Rikha Samba Glacier. Consequently, the model is unable to provide insights into the lateral spatial variability in mass balance across the entire glacier. Additional uncertainty may stem from the off-glacier AWS data used to compute the surface-energy balance of the glacier, as this does not capture the full heterogeneity of the glacier surface and therefore cannot be directly compared to the glacier melt rates (Stigter and others, 2018). Furthermore, the ERA5L data have its own limitations such as a lower spatial resolution when compared to observational data. The model does not include any component of heat sourced from rainfall as this has been previously shown to contribute a minimal amount of energy compared to other radiative and turbulent heat fluxes in the total energy calculations (Kayastha and others, 1999; Mandal and others, 2022). The model also does not account for snow deposition and transport due to topography and wind redistribution, which lowers the accuracy of the mass-balance calculations. Finally, although different glacier area boundaries were used to calculate the glacier-wide mass balance for each decade (1980, 1990, 2000, 2010 and 2020), these glacier boundaries are assumed to remain constant when calculating annual mass balances within each respective decade which limits the accuracy of the annual mass-balance calculations.

### 5. Conclusions

We calculated the annual mass balance of Rikha Samba Glacier from 1974–2021 to fill a large temporal gap in field observations that are available for 1974, 1998/99 and 2011–2021. We also updated the field-based mass-balance measurement until 2021 after the comprehensive documentation of on-going glacier monitoring of this glacier since 2011 (Stumm and others, 2021). We demonstrate that a physically-based energy-mass balance model can reconstruct the surface mass balance of Rikha Samba Glacier using reanalysis ERA5L, AWS, and in situ mass-balance data. The average annual glacier-wide mass balance and cumulative mass balance were found to be –0.56 m w.e. a<sup>–1</sup> from 1974 to 2021. The reconstruction demonstrates that Rikha Samba Glacier had a more negative mass balance (–0.65 m w.e. a<sup>–1</sup>) in the past (1974–2000) compared to the more recent decades (2000–2021, –0.47 w.e. a<sup>–1</sup>). Sensitivity analysis of the input variables to the mass-balance changes, conducted by perturbing the quantity of precipitation, relative humidity and solar radiation by ±20% and air temperature by ±1 K, shows that mass-balance variability is most sensitive to changes in air temperature.

**Supplementary material.** The supplementary material for this article can be found at <https://doi.org/10.1017/jog.2022.93>.

**Acknowledgements.** We thank the Government of Norway for supporting and funding this research, as well as our national partners, including the Department of Hydrology and Meteorology Government of Nepal (DHM), Water and Energy Commission Secretariat, Government of Nepal (WECS), and Tribhuvan University, Nepal (TU). This study was partially supported by core funds of ICIMOD contributed by the governments of Afghanistan, Australia, Austria, Bangladesh, Bhutan, China, India, Myanmar, Nepal, Norway, Pakistan, Sweden and Switzerland. We acknowledge Tenzing Chogyal Sherpa for making the study area map and his contribution to mass-balance measurement in 2018 along with Dawa Tshering Sherpa. The authors extend a big thanks to all field members, field assistants, porters, guides and special gratitude to Ang Kipa Sherpa, Chyapten Sherpa, Laxmi Kumar Rai and Pemba Sherpa for their support during the glacier measurements, installation and maintenance of weather station and for all of their logistical support. We extend our sincere gratitude to Dorothea Stumm, Bikas Bhattarai, Niraj Pradhananga for the initial mass-balance stake and weather station installation and maintenance, and for their intellectual support. K. Fujita was supported by JSPS-KAKENHI (grant numbers 17H01621 and 18KK0098), and JSPS and SNSF under the Joint Research Projects (JRPs). Finally, we thank the scientific editor, Argha Banerjee, and two anonymous reviewers for thorough and helpful reviews that significantly improved the paper.

**Author contributions.** T.R.G. and R.B.K. designed the study. T.R.G., J.D.K. and S.P.J. analyzed the data. T.R.G. performed model calculation with the support of K.F. T.R.G., S.P.J., A.S. and K.F. conducted field visits in different periods. T.R.G. wrote the manuscript with the support of all other co-authors.

**Data availability statement.** The in situ mass-balance datasets are also available from the World Glacier Monitoring Service (WGMS) compiled and edited by Zemp and others (2021).

**Disclaimer.** The views and interpretations in this publication are those of the authors and are not necessarily attributable to ICIMOD.

## References

- Acharya A and Kayastha RB (2019) Mass and energy balance estimation of Yala Glacier (2011–2017), Langtang Valley, Nepal. *Water* **11**(1), 6. doi: [10.3390/w11010006](https://doi.org/10.3390/w11010006)
- Azam MF and 5 others (2014) Reconstruction of the annual mass balance of Chhota Shigri glacier, Western Himalaya, India, since 1969. *Annals of Glaciology* **55**(66), 69–80. doi: [10.3189/2014AoG66A104](https://doi.org/10.3189/2014AoG66A104)
- Azam MF and 5 others (2018) Review of the status and mass changes of Himalayan-Karakoram glaciers. *Journal of Glaciology* **64**(243), 61–74. doi: [10.1017/jog.2017.86](https://doi.org/10.1017/jog.2017.86)
- Azam F and Srivastava S (2020) Mass balance and runoff modelling of partially debris-covered Dokriani Glacier in monsoon-dominated Himalaya using ERA5 data since 1979. *Journal of Hydrology* **590**, 125432. doi: [10.1016/j.jhydrol.2020.125432](https://doi.org/10.1016/j.jhydrol.2020.125432)
- Bajracharya SR and 6 others (2015) The glaciers of the Hindu Kush Himalayas: current status and observed changes from the 1980s to 2010. *International Journal of Water Resources Development* **31**(2), 161–173. doi: [10.1080/07900627.2015.1005731](https://doi.org/10.1080/07900627.2015.1005731)
- Bolch T and 10 others (2019) Status and change of the cryosphere in the extended Hindu Kush Himalaya Region. In Wester P, Mishra A, Mukherji A and Shrestha AB (eds.), *The Hindu Kush Himalaya Assessment*. Springer: Switzerland, 209–255. doi: [10.1007/978-3-319-92288-1](https://doi.org/10.1007/978-3-319-92288-1)
- Brun F, Berthier E, Wagnon P, Kääb A and Treichler D (2017) A spatially resolved estimate of High Mountain Asia glacier mass balances from 2000 to 2016. *Nature Geoscience* **10**, 668–673. doi: [10.1038/NGEO2999](https://doi.org/10.1038/NGEO2999)
- Che Y and 7 others (2019) Energy balance model of mass balance and its sensitivity to meteorological variability on Urumqi River Glacier No. 1 in the Chinese Tien Shan. *Scientific Reports* **9**(1), 1–13. doi: [10.1038/s41598-019-50398-4](https://doi.org/10.1038/s41598-019-50398-4)
- Fountain AG and Vecchia A (1999) How many stakes are required to measure the mass balance of a glacier? *Geografiska Annaler: Series A, Physical Geography* **81**(4), 563–573. doi: [10.1111/j.0435-3676.1999.00084.x](https://doi.org/10.1111/j.0435-3676.1999.00084.x)
- Fujii Y, Nakawo M and Shrestha M (1976) Mass balance studies of the glaciers in hidden valley, Mukut Himal. *Journal of the Japanese Society of Snow and Ice* **38**(Special), 17–21.
- Fujita K (2008) Influence of precipitation seasonality on glacier mass balance and its sensitivity to climate change. *Annals of Glaciology* **48**, 88–92. doi: [10.1016/j.epsl.2008.08.028](https://doi.org/10.1016/j.epsl.2008.08.028)
- Fujita K and 6 others (2011) Favorable climatic regime for maintaining the present-day geometry of the Gregoriev glacier, inner Tien Shan. *The Cryosphere* **5**(3), 539–549. doi: [10.5194/tc-5-539-2011](https://doi.org/10.5194/tc-5-539-2011)
- Fujita K and Ageta Y (2000) Effect of summer accumulation on glacier mass balance on the Tibetan Plateau revealed by mass-balance model. *Journal of Glaciology* **46**(153), 244–252. doi: [10.3189/172756500781832945](https://doi.org/10.3189/172756500781832945)
- Fujita K, Nakawo M, Fujii Y and Paudyal P (1997) Changes in glaciers in Hidden Valley, Mukut Himal, Nepal Himalayas, from 1974 to 1994. *Journal of Glaciology* **43**(145), 583–588. doi: [10.1017/S002214300003519X](https://doi.org/10.1017/S002214300003519X)
- Fujita K, Nakazawa F and Rana B (2001) Glaciological observations on Rikha Samba Glacier in Hidden Valley, Nepal Himalayas, 1998 and 1999. *Bulletin of Glaciological Research* **18**, 31–35.
- Fujita K and Nuimura T (2011) Spatially heterogeneous wastage of Himalayan glaciers. *Proceedings of the National Academy of Sciences* **108**(34), 14011–14014. doi: [10.1073/pnas.1106242108](https://doi.org/10.1073/pnas.1106242108)
- Fujita K, Ohta T and Ageta Y (2007) Characteristics and climatic sensitivities of runoff from a cold-type glacier on the Tibetan Plateau. *Hydrological Processes* **21**(21), 2882–2891. doi: [10.1002/hyp.6505](https://doi.org/10.1002/hyp.6505)
- Fujita K and Sakai A (2014) Modelling runoff from a Himalayan debris-covered glacier. *Hydrology and Earth System Sciences* **18**(7), 2679–2694. doi: [10.5194/hess-18-2679-2014](https://doi.org/10.5194/hess-18-2679-2014)
- Gardner AS and 15 others (2013) A reconciled estimate of glacier contributions to sea level rise: 2003 to 2009. *Science* **340**(6134), 852–857. doi: [10.1126/science.1234532](https://doi.org/10.1126/science.1234532)
- Gilbert A and 6 others (2020) The influence of water percolation through crevasses on the thermal regime of a Himalayan mountain glacier. *The Cryosphere* **14**(4), 1273–1288. doi: [10.5194/tc-14-1273-2020](https://doi.org/10.5194/tc-14-1273-2020)
- Gurung S and 5 others (2016) Study of annual mass balance (2011–2013) of Rikha. *Sciences in Cold and Arid Regions* **8**(4), 311–318. doi: [10.3724/SP.J.1226.2016.00311](https://doi.org/10.3724/SP.J.1226.2016.00311)
- Higuchi K (1977) Effect of nocturnal precipitation on the mass balance of the Rikha Samba Glacier, Hidden Valley, Nepal. *Journal of the Japanese Society of Snow and Ice* **39**(Special), 43–49.
- Ichiyanagi K, Yamanaka MD, Muraji Y and Vaidya BK (2007) Precipitation in Nepal between 1987 and 1996. *International Journal of Climatology* **27**(13), 1753–1762. doi: [10.1002/joc.1492](https://doi.org/10.1002/joc.1492)
- Immerzeel W, Petersen L, Raetelli S and Pellicciotti F (2014) The importance of observed gradients of air temperature and precipitation for modeling runoff from a glacierized watershed in the Nepalese Himalayas. *Water Resources Research* **50**(3), 2212–2226. doi: [10.1002/2013WR014506](https://doi.org/10.1002/2013WR014506)
- Johnson E and Rupper S (2020) An examination of physical processes that trigger the albedo-feedback on glacier surfaces and implications for regional glacier mass balance across high mountain Asia. *Frontiers in Earth Science*, **8**, 129. doi: [10.3389/feart.2020.00129](https://doi.org/10.3389/feart.2020.00129)
- Kääb A, Berthier E, Nuth C, Gardelle J and Arnaud Y (2012) Contrasting patterns of early twenty-first-century glacier mass change in the Himalayas. *Nature* **488**(7412), 495–498. doi: [10.1038/nature11324](https://doi.org/10.1038/nature11324)
- Kaser G, Cogley JG, Dyurgerov MB, Meier MF and Ohmura A (2006) Mass balance of glaciers and ice caps: consensus estimates for 1961–2004. *Geophysical Research Letters* **33**(19), 1–5. doi: [10.1029/2006GL027511](https://doi.org/10.1029/2006GL027511)
- Kayastha RB, Ohata T and Ageta Y (1999) Application of a mass balance model to a Himalayan Glacier. *Journal of Glaciology* **45**(151), 559–567. doi: [10.3189/S00221430000143X](https://doi.org/10.3189/S00221430000143X)
- Kirkham JD and 8 others (2019) Near real-time measurement of snow water equivalent in the Nepal Himalayas. *Frontiers in Earth Science* **7**, 177. doi: [10.3389/feart.2019.00177](https://doi.org/10.3389/feart.2019.00177)
- Kochendorfer J and 22 others (2017) Analysis of single-Alter-shielded and unshielded measurements of mixed and solid precipitation from WMO-SPICE. *Hydrology and Earth System Sciences* **21**(7), 3525–3542. doi: [10.5194/hess-21-3525-2017](https://doi.org/10.5194/hess-21-3525-2017)
- Kondo J and Yamazawa H (1986) Bulk transfer coefficient over a snow surface. *Boundary-Layer Meteorology* **34**, 123–135. doi: [10.1007/BF00120912](https://doi.org/10.1007/BF00120912)
- Lama L, Kayastha RB, Maharjan SB and Mool PK (2015) Glacier area and volume changes of Hidden Valley, Mustang, Nepal from ~1980s to 2010 based on remote sensing. *Proceedings of the International*

- Association of Hydrological Science* **368**, 57–62. doi: [10.5194/piahs-368-57-2015](https://doi.org/10.5194/piahs-368-57-2015)
- Lin H, Li G, Cuo L, Hooper A and Ye Q** (2017) A decreasing glacier mass balance gradient from the edge of the Upper Tarim Basin to the Karakoram during 2000–2014. *Scientific Reports* **7**(1), 1–9. doi: [10.1038/s41598-017-07133-8](https://doi.org/10.1038/s41598-017-07133-8)
- Litt M and 6 others** (2019) Glacier ablation and temperature indexed melt models in the Nepalese Himalaya. *Scientific Reports* **9**(1), 1–13. doi: [10.1038/s41598-019-41657-5](https://doi.org/10.1038/s41598-019-41657-5)
- Mandal A and 9 others** (2020) Understanding the interrelationships among mass balance, meteorology, discharge and surface velocity on Chhota Shigri Glacier over 2002–2019 using in situ measurements. *Journal of Glaciology* **66**(259), 727–741. doi: [10.1017/jog.2020.42](https://doi.org/10.1017/jog.2020.42)
- Mandal A and 6 others** (2022) An 11-year record of wintertime snow-surface energy balance and sublimation at 4863 m a.s.l. on the Chhota Shigri Glacier moraine (western Himalaya, India). *The Cryosphere*, **16**, 3775–3799. doi: [10.5194/tc-16-3775-2022](https://doi.org/10.5194/tc-16-3775-2022)
- Mekonnen GB, Matula S, Doležal F and Fišák J** (2015) Adjustment to rainfall measurement undercatch with a tipping-bucket rain gauge using ground-level manual gauges. *Meteorology and Atmospheric Physics* **127** (3), 241–256. doi: [10.1007/s00703-014-0355-z](https://doi.org/10.1007/s00703-014-0355-z)
- Muñoz-Sabater J and 16 others** (2021) ERA5-Land: a state-of-the-art global reanalysis dataset for land applications. *Earth System Science Data* **13**(9), 4349–4383. doi: [10.5194/essd-13-4349-2021](https://doi.org/10.5194/essd-13-4349-2021)
- Nakawo M, Fuji Y and Shresha ML** (1976) Water discharge of Rikha Samba Khola in Hidden Valley, Mukut Himal. *Journal of the Japanese Society of Snow and Ice* **38**(Special), 27–30.
- Potocki M and 12 others** (2022) Mt. Everest's highest glacier is a sentinel for accelerating ice loss. *NPJ Climate and Atmospheric Science* **5**(1), 1–8. doi: [10.1038/s41612-022-00230-0](https://doi.org/10.1038/s41612-022-00230-0)
- Rasmussen R and 14 others** (2012) How well are we measuring snow: the NOAA/FAA/NCAR winter precipitation test bed. *Bulletin of the American Meteorological Society* **93**(6), 811–829. doi: [10.1175/BAMS-D-11-00052.1](https://doi.org/10.1175/BAMS-D-11-00052.1)
- Sakai A and 7 others** (2006) Hydrological observations at July 1<sup>st</sup> Glacier in northwest China from 2002 to 2004. *Bulletin of Glaciological Research* **23**, 3.
- Sakai A and 5 others** (2015) Climate regime of Asian glaciers revealed by GAMDAM glacier inventory. *The Cryosphere* **9**(3), 865–880. doi: [10.5194/tc-9-865-2015](https://doi.org/10.5194/tc-9-865-2015)
- Sakai A and Fujita K** (2017) Contrasting glacier responses to recent climate change in high-mountain Asia. *Scientific Reports* **7**(1), 1–8. doi: [10.1038/s41598-017-14256-5](https://doi.org/10.1038/s41598-017-14256-5)
- Sakai A, Fujita K, Nakawo M and Yao T** (2009) Simplification of heat balance calculation and its application to the glacier runoff from the July 1st Glacier in northwest China since the 1930s. *Hydrological Processes* **23**(4), 585–596. doi: [10.1002/hyp.7187](https://doi.org/10.1002/hyp.7187)
- Sauter T and Oblitner F** (2015) Assessing the uncertainty of glacier mass-balance simulations in the European Arctic based on variance decomposition. *Geoscientific Model Development* **8**(12), 3911–3928. doi: [10.5194/gmd-8-3911-2015](https://doi.org/10.5194/gmd-8-3911-2015)
- Sevruck B, Hertig, JA and Spiess R** (1991) The effect of a precipitation gauge orifice rim on the wind field deformation as investigated in a wind tunnel. *Atmospheric Environment. Part A. General Topics* **25**(7), 1173–1179. doi: [10.1016/0960-1686\(91\)90228-Y](https://doi.org/10.1016/0960-1686(91)90228-Y)
- Shea JM and 5 others** (2015) A comparative high-altitude meteorological analysis from three catchments in the Nepalese Himalaya. *International Journal of Water Resources Development* **31**(2), 174–200. doi: [10.1080/07900627.2015.1020417](https://doi.org/10.1080/07900627.2015.1020417)
- Shean DE and 5 others** (2020) A systematic, regional assessment of high mountain Asia glacier mass balance. *Frontiers in Earth Science* **7**, 363. doi: [10.3389/feart.2019.00363](https://doi.org/10.3389/feart.2019.00363)
- Sherpa SF and 8 others** (2017) Contrasted surface mass balances of debris-free glaciers observed between the southern and the inner parts of the Everest region (2007–15). *Journal of Glaciology* **63**(240), 637–651. doi: [10.1017/jog.2017.30](https://doi.org/10.1017/jog.2017.30)
- Shrestha ML, Fujii Y and Nakawo M** (1976) Climate of hidden during the monsoon Mukut Himal in 1974. *Journal of the Japanese Society of Snow and Ice* **38**(Special), 105–108.
- Soheb M and 5 others** (2020) Mass-balance observation, reconstruction and sensitivity of Stok glacier, Ladakh region, India, between 1978 and 2019. *Journal of Glaciology* **66**(258), 627–642. doi: [10.1017/jog.2020.34](https://doi.org/10.1017/jog.2020.34)
- Srivastava S and Azam MF** (2022) Mass- and energy-balance modelling, and sublimation losses on Dokriani Bamak and Chhota Shigri glaciers in Himalaya since 1979. *Frontiers in Water* **4**, 874240. doi: [10.3389/frwa.2022.874240](https://doi.org/10.3389/frwa.2022.874240)
- Stigter E and 6 others** (2018) The importance of snow sublimation on a Himalayan glacier. *Frontiers in Earth Science* **6**, 108. doi: [10.3389/feart.2018.00108](https://doi.org/10.3389/feart.2018.00108)
- Stumm D, Joshi SP, Gurung TR and Silwal G** (2021) Mass balances of Yala and Rikha Samba glaciers, Nepal, from 2000 to 2017. *Earth System Science Data* **13**(8), 3791–3818. doi: [10.5194/essd-13-3791-2021](https://doi.org/10.5194/essd-13-3791-2021)
- Sunako S, Fujita K, Sakai A and Kayastha RB** (2019) Mass balance of Trambau Glacier, Rolwaling region, Nepal Himalaya: in-situ observations, long-term reconstruction and mass-balance sensitivity. *Journal of Glaciology* **65**(252), 605–616. doi: [10.1017/jog.2019.37](https://doi.org/10.1017/jog.2019.37)
- Thayyen RJ and Dimri AP** (2018) Slope environmental lapse rate (SELR) of temperature in the monsoon regime of the Western Himalaya. *Frontiers in Environmental Science* **6**, 42. doi: [10.3389/fevns.2018.00042](https://doi.org/10.3389/fevns.2018.00042)
- Ueno K and 7 others** (1994) Characteristics of precipitation distribution in Tanggula, Monsoon, 1993. *Bulletin of Glacier Research* **12**, 39–47.
- Wagnon P and 10 others** (2007) Four years of mass balance on Chhota Shigri Glacier, Himachal Pradesh, India, a new benchmark glacier in the western Himalaya. *Journal of Glaciology* **53**(183), 603–611. doi: [10.3189/002214307784409306](https://doi.org/10.3189/002214307784409306)
- Wagnon P and 11 others** (2013) Seasonal and annual mass balances of Mera and Pokalde glaciers (Nepal Himalaya) since 2007. *The Cryosphere* **7**(6), 1769–1786. doi: [10.5194/tc-7-1769-2013](https://doi.org/10.5194/tc-7-1769-2013)
- Wagnon P and 10 others** (2020) Reanalysing the 2007–19 glaciological mass-balance series of Mera Glacier, Nepal, Central Himalaya, using geodetic mass balance. *Journal of Glaciology* **67**(261), 117–125. doi: [10.1017/jog.2020.88](https://doi.org/10.1017/jog.2020.88)
- Wolff MA and 5 others** (2015) Derivation of a new continuous adjustment function for correcting wind-induced loss of solid precipitation: results of a Norwegian field study. *Hydrology and Earth System Sciences* **19**(2), 951–967. doi: [10.5194/hess-19-951-2015](https://doi.org/10.5194/hess-19-951-2015)
- Yamaguchi S and Fujita K** (2013) Modeling glacier behavior under different precipitation seasonality. *Arctic, Antarctic, and Alpine Research* **45**(1), 143–152. doi: [10.1657/1938-4246-45.1.143](https://doi.org/10.1657/1938-4246-45.1.143)
- Yang D, Barry G and John M** (1998) Accuracy of NWS 8" standard nonrecording precipitation gauge : results and application of WMO intercomparison. *Journal of Atmospheric and Oceanic Technology* **15**(1), 54–68. doi: [10.1175/1520-0426\(1998\)015<0054:AONSNP>2.0.CO;2](https://doi.org/10.1175/1520-0426(1998)015<0054:AONSNP>2.0.CO;2)
- Ye B, Yang D, Ding Y, Han T and Koike T** (2004) A bias-corrected precipitation climatology for China. *Journal of Hydrometeorology* **5**(6), 1147–1160. doi: [10.1175/JHM-366.1](https://doi.org/10.1175/JHM-366.1)
- Zandbergen P** (2008) Applications of shuttle radar topography mission elevation data. *Geography Compass* **2**(5), 1404–1431. doi: [10.1111/j.1749-8198.2008.00154.x](https://doi.org/10.1111/j.1749-8198.2008.00154.x)
- Zemp M and 14 others** (2019) Global glacier mass changes and their contributions to sea-level rise from 1961 to 2016. *Nature* **568**(7752), 382–386. doi: [10.1038/s41586-019-1071-0](https://doi.org/10.1038/s41586-019-1071-0)
- Zemp M and 6 others** (2021) Global glacier change bulletin No. 4 (2018–2019). *Global Glacier Change Bulletin* **4**, 278. doi: [10.5904/wgms-fog-2021-05](https://doi.org/10.5904/wgms-fog-2021-05)
- Zhang G and 10 others** (2013) Energy and mass balance of Zhadang glacier surface, central Tibetan Plateau. *Journal of Glaciology* **59**(213), 137–148. doi: [10.3189/2013JoG12J152](https://doi.org/10.3189/2013JoG12J152)
- Zhao H, Yang W, Yao T, Tian L and Xu B** (2016) Dramatic mass loss in extreme high-elevation areas of a western Himalayan glacier: observations and modeling. *Scientific Reports* **6**, 30706. doi: [10.1038/srep30706](https://doi.org/10.1038/srep30706)
- Zhu M and 5 others** (2021) The influence of key climate variables on mass balance of Naimona'nyi Glacier on a north-facing slope in the western Himalayas. *Journal of Geophysical Research: Atmospheres* **126**(7), e2020JD033956. doi: [10.1029/2020JD033956](https://doi.org/10.1029/2020JD033956)